On the Interest of Bulk Conductivity Measurements for Hydraulic Dispersivity Estimation from Miscible Displacement Experiments in Rock Samples

Alexis Maineult, Jean-Baptiste Clavaud, Maria Zamora

TECHNICAL NOTE

On the interest of bulk conductivity measurements for hydraulic dispersivity estimation from miscible displacement experiments in rock samples.

Alexis Maineult [1,2,+], Jean-Baptiste Clavaud [1,*] and Maria Zamora [1]

1) Institut de Physique du Globe de Paris, Sorbonne Paris Cité, Univ Paris Diderot, UMR 7154 CNRS, 1 rue Jussieu, 75005 Paris, France

2) Sorbonne Universités, UPMC Univ Paris 06, CNRS, EPHE, UMR 7619 Metis, 4 place Jussieu, 75005 Paris, France

[*] *now at Chevron Energy Technology Company, 1500 Louisiana St., Houston, TX 77002, USA*

[+] *corresponding author. Phone*: +33 (0)1 44 27 43 36. *E-mail address*: *alexis.maineult@upmc.fr*

SUMMARY

The determination of the hydraulic dispersivity and effective fraction of porous medium contributing to transport on soil and rock sample in the laboratory is important to understand and model the evolution of miscible contaminant plumes in groundwater. Classical methods are based on the interpretation of the breakthrough curve, i.e., the evolution of the concentration in contaminant at the downstream end-face of a sample into which a front of contaminant is advected. Here we present an experimental device aimed at performing such measurements, but also allowing the bulk electrical conductivity of the sample to be measured. We show that the dispersivity and effective fraction can be inferred from this electrical measurement, and that the combined use of both out-flowing fluid conductivity and bulk conductivity allows the incertitude on the dispersivity and effective fraction to be significantly enhanced.

Keywords: miscible displacement, hydraulic dispersivity, breakthrough curve, electrical conductivity

1. Introduction

Miscible contaminants flowing through a porous medium by advection are mixing with the non-contaminated water, yielding to dilution of the plume. This so-called dispersion phenomenon originates from the fact that the fluid moves faster in larger pores than in smaller ones and faster in the centres of the pores than along the walls, and also that some pathways are longer than others (e.g., Fetter 2001). If we consider an isotropic and homogeneous soil or rock sample, and assume that i) the flow through it is purely one-dimensional and ii) the dispersion process is Fickian, the concentration field $C(x,t)$ (in $\mathrm{mol\,m^{-3}}$) inside the sample, where x (in m) stands for the distance from the upstream-face of the sample and t (in s) for the elapsed time, obeys the transport equation:

$$\frac{\partial C}{\partial t} = D\frac{\partial^2 C}{\partial x^2} - v\frac{\partial C}{\partial x}, \tag{1}$$

Here D is the hydrodynamic dispersion coefficient (in $\mathrm{m^2\,s^{-1}}$) and v the linear average velocity of water flowing through the sample (in $\mathrm{m\,s^{-1}}$). Provided that diffusion processes can be neglected, the dispersion coefficient in Eq. (1) can be written $D = \lambda v$, where λ is the hydraulic dispersivity (in m). Even though the dispersivity changes with the observation scale (e.g., Xu and Epstein 1995), it is often required to determine its value on soil or rock samples to understand and model the dynamics of contaminants at the field scale.

The classical way to perform such measurements in the laboratory consists in applying a straight front of salty solution at the entrance (i.e., the upstream face) of the sample subjected to permanent, laminar flow, and to measure the concentration at the outlet (i.e., the downstream face). The evolution of the concentration of the out-flowing fluid, or "breakthrough curve", is generally sigmoidal, provided that the medium is homogeneous at the scale of the sample and

55 that no other processes occur, such as chemical reactions with the minerals. The spreading of the
56 curve increases with the dispersivity. Knowing the theoretical formulation of the breakthrough
57 curve, it is then possible to determine the value of the dispersivity by fitting methods.

58 The out-flowing concentration is an integrated value, which presents variations only when
59 the salt front reaches the downstream face of the sample. Other methods, such as electrical
60 measurements, can give information as soon as the salt front penetrates the sample. For example,
61 Odling et al. (2007) used electrical impedance measurements on microfractured granite to
62 determine its longitudinal dispersivity. They showed that such a technique provided supplemental
63 information about the dispersion process inside the sample. Here we report on an apparatus
64 allowing the bulk conductivity of a rock sample to be measured during miscible displacement
65 experiments. We show that fitting the classical breakthrough curve to the measured electrical
66 conductivity of the out-flowing fluid, combined to fitting the theoretical evolution of the bulk
67 conductivity of the sample to the measured one, enables a more accurate determination of the
68 hydraulic dispersivity and fraction of the porous volume effectively contributing to the transport.
69

70 **2. Materials and method**

71

72 *2.1. Device and procedure*

73 We devised, constructed and tested an experimental set-up (Fig. 1), aimed at measuring
74 the bulk electrical conductivity σ_b (in S m^{-1}) of large-sized samples (i.e., about 5 to 10 cm in
75 diameter and 10-40 cm or more in length), as well as the electrical conductivity of the fluid that is
76 out-flowing from the sample, denoted σ_f. This device is usable to perform miscible displacement
77 experiments and therefore infer the hydraulic dispersivity λ (in m) and the effective fraction of

78 the porous volume contributing to transport, denoted f (no unit).

79 The upstream and downstream end-faces of the sample, which is placed horizontally to
80 avoid the influence of gravity, are connected to a hydraulic circuit. They are also in perfect
81 contact with stainless steel electrodes, whose external side is protected by a PVC cap to ensure
82 electrical isolation. The conductivity of the out-flowing fluid is measured with a custom-made
83 cell with four platinum electrodes that was calibrated with various brines at different frequencies.
84 The fluid conductivity and the bulk conductivity of the sample are measured with an impedance-
85 meter HP 4263A, at the frequencies of 120 and 1000 Hz. The optimal frequency, which
86 minimizes the polarization effects, is equal to 1 kHz. Note that concerning the bulk conductivity,
87 the measure is done with the two electrodes at the end-faces of the sample only, each electrode
88 serving for both current injection and potential measurement.

89 To check its watertightness, the sample is first put under vacuum for a few hours. The
90 sample is then saturated with distilled and de-aerated water. The porosity accessible by water
91 under vacuum, which is close to the connected porosity, is deduced from the amount of injected
92 water required to fill the connected voids, with an accuracy comprised between 0.3 and 3.5
93 percents. Then we let the fluid flowing through the sample from the upstream reservoir filled
94 with distilled water. Once the chemical equilibrium is reached, i.e. when the conductivity of the
95 out-flowing fluid is constant, the distilled water saturating the sample is flushed by NaCl brine at
96 a concentration around 3 $\mathrm{g\,L^{-1}}$, coming from the brine reservoir. This value of the concentration
97 is large enough to consider the contribution of the surface conduction to the total electrical
98 conductivity negligible, but small enough to neglect density-driven flow, at least for highly
99 permeable samples. Brine is injected until the out-flowing solution has the same electrical
100 conductivity. In practice, a given amount of brine is introduced in the sample. The electrical
101 measurements are carried out rapidly enough to neglect the effects of pure diffusion and reduce

102 the density effects, if any. Afterwards we proceed to a new injection step, and so on.

103

104 *2.2 Tested sample*

105 To test our approach, we use a decimetric core of Saint-Maximin limestone (denoted
106 SML). It is a bioclastic limestone, having a large macro-porosity, and a small amount of
107 intraclastic porosity (Fig. 2a). The results of mercury injection carried out on a centimetric core
108 (Fig. 2b) show that the distribution of the pore access radii is bi-modal with to modes at 13.6 and
109 0.13 μm respectively. However, the second mode, which corresponds to the intraclastic porosity,
110 is clearly dominated by the first mode.

111 The sample was 309 mm in length, with a diameter of 97.90 mm. The volume of the
112 sample (2326 cm^3) is therefore two orders of magnitude larger than the volumes of rock samples
113 commonly studied in the laboratory for permeability estimation (i.e., 20 to 50 cm^3). This size was
114 chosen to acquire measurements at a scale significantly larger than the representative elementary
115 volume (e.g., Henriette et al. 1989). After machining, the sample was dried in an oven at 60 °C
116 for several days, until its weight stabilized. Then the lateral surface was waterproofed by
117 covering it with epoxy resin. The connected porosity value, determined from weighting, was
118 equal to 36.6 ± 0.5 %. From flow-rate measurement, the water permeability was estimated to be
119 1718 ± 42 mD.

120 To check if advection is predominant over diffusion in our experiment, we estimated the
121 Péclet number Pe. The classical formulation $Pe = v_{DF}\ d\ /\ D_m$ (e.g., Sahimi 1993), where v_{DF} is the
122 Dupuit-Forcheimer velocity (in $m\ s^{-1}$), d the mean grain diameter (in m) and D_m the molecular
123 diffusion coefficient ($1.5\ 10^{-9}$ $m^2\ s^{-1}$ for NaCl), is not applicable for non-granular rocks.
124 Therefore, we used the non-correlation radius r_{nc}, estimated from image analysis, instead of $d/2$.

This yields to $\mathrm{Pe} = 2\ v_{\mathrm{DF}}\ r_{nc}\ /\ D_m$. For the highly permeable sample SML, v_{DF} was equal to 0.35 mm s^{-1} during the experiment, and r_{nc} was estimated to 175 µm. The Péclet number is thus around 80, meaning that in this case advection can be neglected (power-law regime, e.g. Sahimi 1993).

For the miscible displacement experiment, the conductivity of the initial fluid after stabilization was equal to 4.7 mS m^{-1}. The conductivity of the injected fluid was 540 mS m^{-1}. (i.e., 54.3 mmol L^{-1} or 3.17 g L^{-1} NaCl). The bulk conductivity of the sample was equal to 1.4 mS m^{-1} initially, and to 90.1 mS m^{-1} at the end of the experiment, yielding to an electrical formation factor $F = \sigma_f / \sigma_b$ equal to 6.

3. Theory

3.1. Problem and solution for a 1D isotropic and homogeneous medium

Considering that Eq. (1) applies to our case, the initial condition is $C(x,0) = C_0$, where C_0 is the equivalent salt concentration of the solution initially saturating the pore space. The upstream boundary condition, corresponding to the injection of brine starting at $t = 0$, can be formalized as $C(0,t) = C_0 + (C_{\mathrm{brine}} - C_0)\,\mathrm{H}(t)$ where C_{brine} is the concentration of the brine and H the Heaviside step function. The solution is given by (e.g., Ogata and Banks 1961; Fried and Combarnous 1971; Gupta and Greenkorn 1974; Basak and Murty 1979):

$$C(x,t) = C_0 + \frac{C_{\mathrm{brine}} - C_0}{2}\left[\mathrm{erfc}\left(\frac{x - vt}{2\sqrt{Dt}}\right) + \exp\left(\frac{vx}{D}\right)\mathrm{erfc}\left(\frac{x + vt}{2\sqrt{Dt}}\right)\right], \quad (2)$$

where erfc is the complementary error function. The second term in the brackets has an influence only if t is close to 0, and can be neglected otherwise (e.g., Ogata and Banks 1961; Pfannkuch 1963), yielding to the following approximation of Eq. (2):

$$C(x,t) \approx C_0 + \frac{C_{\text{brine}} - C_0}{2} \operatorname{erfc}\left(\frac{x - vt}{2\sqrt{Dt}} \right). \quad (3)$$

3.2. Non-dimensionalization of the solution

In order to compare the breakthrough curves for different samples, if any, it is convenient to use the normalized variation of the concentration δC (no unit) defined by

$$\delta C(x,t) = \frac{C(x,t) - C_0}{C_{\text{brine}} - C_0}. \quad (4)$$

Since the injection is not continuous but performed step by step (see end of section 2.1), it is convenient to consider δC as a function of the normalized injected volume of brine V_i^n, expressed in pore volumes, as (e.g., Pickens and Grisak 1981):

$$V_i^n = \frac{V_i}{V_{pc}}, \quad (5)$$

where V_i is the injected volume of brine and V_{pc} the total connected porous volume of the sample, equal to the total porosity times the volume of the sample. Following this way, the curves δC versus V_i^n for different samples are similarly scaled and therefore directly comparable. Indeed, the time required for the injection of a given volume of brine, which depends on the permeability of the rock, is eliminated from Eq. (3): considering that V_i^n is also equal to $v\,t\,/\,L$ where L is the length of the sample (in m), and assuming that the molecular diffusion is negligible so that we can introduce the hydraulic dispersivity as $\lambda = D\,/\,v$, the combination of Eqs. (3) and (4) leads to:

$$\delta C(x,t) \approx \frac{1}{2} \operatorname{erfc}\left(\frac{1}{2} \sqrt{\frac{L}{\lambda}} \frac{\left(\frac{x}{L} - V_i^n \right)}{\sqrt{V_i^n}} \right). \quad (6)$$

The normalized variation of concentration of the out-flowing solution, denoted δC_{out}, is obtained

by taking $x = L$ in Eq. (6):

$$\delta C_{out}(t) = \delta C(L,t) \approx \frac{1}{2}\operatorname{erfc}\left(\frac{1}{2}\sqrt{\frac{L}{\lambda}}\frac{1-V_i^n}{\sqrt{V_i^n}}\right) \tag{7}$$

Classically, the λ / L ratio is inferred from the measured values of δC_{out} (i.e., the normalized breakthrough curve) by fitting the theoretical curve (Eq. (7)) to them. Note here that this theoretical curve passes through the point $M_{1,0.5} = (V_i^n, \delta C_{out}) = (1,0.5)$, since the volume of brine required for the centre of mass of the front to arrive at the downstream end of the sample is equal to one pore volume.

It is assumed here that the whole connected pore volume contributes to the transport, but it is rarely expected. For example, dead-end pores do not contribute to the transport processes. If the pore volume contributing to transport (or "efficient porosity"), denoted V_{pc}^*, is smaller than V_{pc}, the experimental curve δC_{out} versus V_i^n is shifted to the left. In other words, the injected volume, normalized using Eq. (5), for which δC_{out} is equal to 0.5, is smaller than 1. In this case, one should also find the best V_{pc}^* to be used in place of V_{pc} in Eq. (5). To do so, we define the effective fraction of the porous volume contributing to the transport as $f = V_{pc}^*/V_{pc}$. Equation (5) must thus be rewritten as:

$$V_i^n = \frac{V_i}{V_{pc}^*} = \frac{V_i}{fV_{pc}}. \tag{8}$$

The problem then involves two parameters, λ/L and f, to be found using Eqs. (7) and (8).

It should be noted here that if no theoretical curve can explain the data, it means that the medium is not homogeneous, and/or that retardation processes occur such as trapping in small pores, or that molecular diffusion is not negligible, or that density-driven flow occurs, or even chemical reactions with the reactive mineral phases happen.

Finally, note that for the calculation of V_i^n, the measured injected volume of brine was corrected from the volume of the tube between the T-valve (Fig. 1) and the upstream end of the sample for the bulk sample conductivity, and from the same volume plus the volume of the tube between the downstream end of the sample and the conductivity cell for the conductivity of the out-flowing fluid.

3.3. Conversion of conductivity to concentration

As previously stated, we do not measure the salt concentration directly, but the electrical conductivity of the fluid. To transform the concentration C into conductivity σ_f, and reciprocally σ_f into C, we use the empirical relations established by Sen and Goode (1992) for NaCl brine:

$$\sigma_f = \left(5.6 + 0.27T - 1.5\,10^{-4}T^2\right)M - \frac{2.36 + 0.099T}{1 + 0.214M}M^{\frac{3}{2}} \tag{9}$$

where T is the temperature (in °C) and M is the molality (in $\mathrm{mol\,kg^{-1}}$). To convert the concentration C_f into molality, we use the CRC Handbook Table at 20°C (Lide 2008).

For coherence, we also normalized the conductivity of the out-flowing fluid, σ_{out}, as:

$$\delta\sigma_{out}(t) = \frac{\sigma_{out}(t) - \sigma_{out,0}}{\sigma_{out,\max} - \sigma_{out,0}}, \tag{10}$$

where $\sigma_{out,0}$ and $\sigma_{out,\max}$ are the initial and maximal (i.e., the plateau value at the end of the experiment) conductivities of the effluent solution, respectively. We proceeded similarly for the bulk conductivity of the sample σ_b:

$$\delta\sigma_b(t) = \frac{\sigma_b(t) - \sigma_{b,0}}{\sigma_{b,\max} - \sigma_{b,0}}, \tag{11}$$

where $\sigma_{b,0}$ is the initial and $\sigma_{b,\max}$ the maximal (i.e., the plateau value at the end of the experiment) value of the bulk conductivity.

209

210 **4. Estimation of the dispersivity**

211 To estimate the dispersivity λ, we first use the classical method, which consists in fitting a
212 straight line in Henry's space to the experimental points of the out-flowing fluid concentration.
213 Secondly we systematically explored the parameter space. This second method allows the
214 effective fraction f to be taken into account, and the sample conductivity to be also considered.

215

216 *4.1. Cost-function*

217 To evaluate the agreement between the data (i.e., the normalized measured conductivity
218 variations) and the model (i.e., the normalized predicted conductivity variations), a cost-function
219 R as meaningful as possible has to be defined. We used the determination coefficient r^2, which
220 quantifies the mean deviation of the N experimental points (vector $\mathbf{d}^{\text{obs}}$) from the predictions
221 (vector $\mathbf{d}^{\text{pred}}$):

222
$$r^2 = 1 - \frac{\sum_{i=1}^{N} \left(d^{\text{obs}}{}_i - d^{\text{pred}}{}_i \right)^2}{\sum_{i=1}^{N} \left(d^{\text{obs}}{}_i - \left\langle \mathbf{d}^{\text{obs}} \right\rangle \right)^2} \tag{12}$$

223 Moreover, considering that the concentration break-through curves (Eq. (7)) are similar to
224 cumulative Gaussian distributions, we combined r^2 with the Kolmogorov-Smirnov (KS) test (e.g.,
225 Press et al. 1997), usually used as an estimator of the semblance between two distributions, given
226 by:

227
$$\begin{cases} \mu = \left(\sqrt{N} + 0.12 + \dfrac{0.11}{\sqrt{N}} \right) \max \left| \mathbf{d}^{pred} - \mathbf{d}^{obs} \right| \\ KS = 2 \sum_{j=1}^{\infty} (-1)^{j-1} e^{-2 j^2 \mu^2} \end{cases} \tag{13}$$

228 We thus used the function $R = KS\,r^2$; an optimal fit is obtained when $R = 1$.

229

230 *4.2. Fitting method in Henry's space*

231 Defining the two parameters α (no unit) and Γ (no unit) as:

232 $$\begin{cases} \alpha = \dfrac{1}{2}\sqrt{\dfrac{L}{\lambda}} \\ \Gamma = \dfrac{1 - V_i^n}{\sqrt{V_i^n}} \end{cases}, \tag{14}$$

233 Eq. (7) can be rewritten as:

234 $$\delta C_{out}(t) = \frac{1}{2}\operatorname{erfc}(\alpha\Gamma). \tag{15}$$

235 Therefore the curve Γ versus δC_{out} plotted in linear arithmetic probability paper (in ordinates)
236 forms a straight line (e.g., Brigham 1974), also called Henry's line. The slope of this line,
237 denoted p, is theoretically given by:

238 $$p = -\frac{1}{\alpha\sqrt{2}} = -\sqrt{2}\sqrt{\frac{\lambda}{L}}. \tag{16}$$

239 We did not apply the classical two-point Taylor's (1953) method to determine λ (e.g., Fried and
240 Combarnous 1971; Gupta and Greenkorn 1974; Pickens and Grisak 1981). Instead, we
241 determined the straight line fitting the data in the least-square sense, as suggested by Gupta and
242 Greenkorn (1974), considering that this method provides more accurate values for the slope p.
243 Note that in this case it is necessary to restrict the data to the interval for which the conductivity
244 variation is linear, i.e., generally for δC_{out} comprised between 0.1 and 0.9. The dispersivity is then
245 deduced using Eq. (16) as $\lambda = L\,p^2 / 2$.

246 The observed normalized conductivity $\delta\sigma_{out}$ and deduced normalized concentration δC_{out}
247 of the out-flowing fluid as a function of the volume of injected brine V_i^n, expressed in fraction of

porous volume, are shown in Fig. 3a for SML sample. The concentrations δC_{out} are distributed along a sigmoid, which seems to pass very close to the point $M_{1,0.5} = (V_i^n, \delta C_{out}) = (1,0.5)$, meaning that the whole pore volume contribute to the transport. The associated Γ values computed using Eq. (14), versus normalized experimental concentration δC_{out}, are distributed along a straight line (Fig. 3b). The line fitting the best the data, in the least-squares sense, passes through the point $(\delta C_{out}, \Gamma) = (0.5,0)$, meaning that indeed the effective fraction f is equal to 1. The slope of the fitting line gives a value of 4.018 mm for the dispersivity λ_{HL}. The modelled curves δC_{out} (continuous line in Fig. 3a, obtained with Eqs. (7) and (5)) and $\delta\sigma_{out}$ (dotted line) versus the volume of injected brine, expressed in fraction of porous volume, explain the data rather well (the cost-function R^{HL} is close to 1.0).

4.3. Parameter space exploration

The previous procedure takes into account the conductivity variation of the out-flowing fluid only. Moreover, it does not provide a confidence interval for the dispersivity or the effective fraction of porous volume. We hereafter estimate the dispersivity directly from the curves of the out-flowing fluid conductivity variations $\delta\sigma_{out}$ or/and the variations of the bulk conductivity $\delta\sigma_b$ versus the injected volume V_i^n by exploring the parameter space

To estimate the sample bulk conductivity σ_b, we apply the generalized Reuss average, since the measurement is performed in the direction of the concentration gradient. We assume that i) the concentration front is one-dimensional along the axis of the sample (i.e., the sample is homogeneous and the front is straight, i.e., the density effect are negligible), and ii) the formation factor F does not depend on the value of the local fluid conductivity. Therefore, σ_b can be written as (Odling et al. 2007):

$$\frac{1}{\sigma_b(t)} = \frac{F}{L}\int_0^L \frac{dx}{\sigma_f\left(C(x,t)\right)} \quad (17)$$

where $\sigma_f(C(x,t))$ corresponds to the fluid conductivity distribution inside the sample (computed using Eqs. (3) and (9)). It is important to note that the knowledge of the formation factor is not required, since it vanishes in the computation of the normalized variation of the bulk conductivity using Eq. (11).

The application to limestone SML is shown in Figs. 4, 5 and 6. We explored the dispersivity values in the interval comprised between 0 and 20 mm (based on the value previously determined for λ_{HL},) with a spacing of 0.1 mm, and the values of the effective fraction in the interval comprised between 0.85 and 1 with a spacing of 0.001.

When the exploration method is applied to the fluid conductivity only (Fig. 4a), the maximal value of the cost-function $R^f_{\max}$ is equal to 0.99951 (with a Kolmogorov-Smirnov value equal to 100 %) and corresponds to a dispersivity λ_f (subscript "*f*" standing for "fluid") of 4.0 mm and an effective fraction f_f of 0.982. The value of the dispersivity is very close to the value determined previously using Henry's line (4.018 mm). The value of the effective fraction is very close to 1, but is slightly smaller. The predictions computed with Eqs. (7), (8) and (10) explain very well the data (Fig. 4b).

We proceeded similarly for the bulk conductivity only (Fig. 5). As for the fluid, the normalized bulk conductivity of the sample is sigmoidal, but the bulk conductivity evolves as soon as brine is injected in the sample (Fig. 5b). The dispersivity λ_s (subscript "*s*" standing for "sample") is equal to 3.3 mm, a value slightly smaller than λ_f. The effective fraction f_s is equal to 0.987. The prediction, computed using Eqs. (3), (9), (11) and (17), explains here again rather well the data, with a cost-function $R^s_{\max}$ equal to 0.99954. However, it seems that the dispersivity may

293 be slightly underestimated for injected volume above 1, the prediction being systematically
294 higher than the experimental points.

295 We finally apply the same methodology to find the best dispersivity and effective fraction
296 explaining both fluid and sample conductivities simultaneously (Fig. 6). In this case, we defined
297 the cost-function as the product of the two cost-functions for the fluid and the sample, i.e.
298 $R = R^f R^s$. Doing so, the best dispersivity value λ is equal to 3.5 mm and the best effective
299 fraction f to 0.986 (Fig. 6a). The predictions explained rather well the fluid conductivity (Fig. 6b)
300 and the bulk conductivity of the sample (Fig. 6c).

301

302 **5. Discussion**

303 First of all, a coherent estimation of the dispersivity and of the effective fraction is
304 provided by the interpretation of the evolution of the bulk conductivity of the sample.

305 Secondly, when performing sensitivity analysis, it can be seen that the ranges of
306 dispersivity and effective fraction which produce high values of the cost-function for the out-
307 flowing fluid conductivity are quite large (red area in Fig. 4a). For instance, values of dispersivity
308 between 1.5 and 8.1 and effective fraction between 0.941 and 1 produce a cost-function value
309 superior to 0.99, sufficiently high to produce satisfactorily predictions. A way to estimate the
310 error interval on the determined values of dispersivity and effective fraction may be to consider
311 their values which produce cost-function values higher than a certain threshold value. Here we
312 can consider $R^f = 0.998$. In this case, the dispersivity λ_f is comprised between 3 and 5.4, and the
313 effective fraction f_f between 0.966 and 0.998. From the exploration of the parameter space for the
314 bulk conductivity of the sample, it can be concluded that the bulk conductivity is more sensitive
315 to the variations of the dispersivity (the red area in Fig. 5a is less extended in the λ-direction than

316 in Fig. 4a), but is less sensitive to the variations of the effective fraction (the red area is more
317 extended in the f-direction). Considering again the threshold value of 0.998 for R^s, the
318 dispersivity λ_s is comprised between 2.2 and 4.5, and the effective fraction f_f between 0.955 and
319 1. The dispersivity is thus best determined by the bulk conductivity and the effective fraction by
320 the out-flowing fluid conductivity. This illustrates the fact that using the bulk conductivity of the
321 sample provides supplemental information, compared to the use of the out-flowing fluid
322 conductivity alone. Finally, when considering the exploration on both out-flowing fluid
323 conductivity and bulk conductivity of the sample, the area producing high values of the cost-
324 function R is much restrained than in the previous two cases. Indeed, the $R = 0.998$ threshold
325 gives an interval of [3.2,3.9] for the dispersivity λ and an interval of [0.978,0.994] for the
326 effective fraction f.

327 The fact that the effective fraction is not equal to 1, but close to it, means that a small part
328 of the porous volume does not contribute to the transport. This non-contributing volume may be
329 the intraclastic porosity associated with the second mode in the pore access radius distribution
330 (Fig. 2b). Moreover, the fact that the predictions are slightly higher than the observations for
331 injected volume greater than 1 (Figs. 4b, 5b and 6bc) may be results from retardation processes of
332 small intensity – maybe the penetration of salt in this intraclastic porosity.

333 Finally, the fact that all the estimated dispersivities λ_{HL}, λ_f, λ_s and λ, as well as the
334 effective fractions f_f, f_s and f are close one to the other, and that the data are rather well explained
335 by these values, means that all the assumptions made here (mainly: the sample is homogeneous
336 and the diffusion and the density effect can be neglected) are reasonable. For less permeable
337 samples with lower Péclet number, and/or for higher brine concentration, more complicated
338 models have to be implemented, but this is beyond the scope of this study.

6. Conclusions

We added to the classical measurement of the breakthrough curve (evolution of the conductivity of the out-flowing fluid) during miscible displacements experiments the measurement of the evolution of the bulk conductivity of the sample. A methodology based on the exploration of the possible values for the hydraulic dispersivity and for the effective fraction of total connected porous volume contributing to the transport was developed, which also provide confidence intervals The values obtained on a sample of limestone using the out-flowing fluid conductivity only or the bulk conductivity of the sample only are coherent with those determined by the classical method of Henry line. The most interesting point is that the combined use of out-flowing fluid and bulk conductivities also produces coherent values, but with significantly reduced confidence intervals. This underlines the interest of systematically including the measurement of the bulk conductivity during laboratory measurements of the dispersivity on rock samples.

Acknowledgments

The authors thank all the anonymous reviewers of this work for their helpful comments. This is IPGP contribution n°3744.

References

Basak, P., Murty, V.V.N.: Determination of hydrodynamic dispersion coefficients using "inverfc". J. Hydrol. 41, 43–48 (1979)

Brigham, W.E.: Mixing equations in short laboratory columns. Soc. Pet. Eng. J. 14, 91–99 (1974)

Fetter, C.W.: Applied Hydrogeolgy, 4th Edition. Prentice Hall, NJ (2001)

Fried, J.J., Combarnous, M.A.: Dispersion in porous media. Adv. Hydrosci. 7, 169–282 (1971).

Gupta, S.P., Greenkorn, R.A.: Determination of dispersion and nonlinear adsorption parameters for flow in porous media. Water. Resources Res. 10, 839–846 (1974)

Henriette, A., Jacquin, C.G., Adler, P.M.: The effective permeability of heterogeneous porous media. Physicochem. Hydrodyn. 11, 63–80 (1989)

Lide, D.R. (ed): Handbook of chemistry and physics, 89th edition. CRC Press, Boca Raton, FL (2008)

Odling, N.W.A., Elphick, S.C., Meredith, P., Main, I., Ngwenya, B.T.: Laboratory measurement of hydrodynamic saline dispersion within a micro-fracture network induced in granite. Earth Planet. Sci. Lett. 260, 407–418 (2007)

Ogata, A., Banks, R.B.: A solution of the differential equation of longitudinal dispersion in porous media. U.S. Geol. Surv. Professionnal Paper, 411-A (1961)

Pfannkuch, H.O.: Contribution à l'étude des déplacements de fluides miscibles dans un milieu poreux. Rev. Inst. Fr. Pét. 18, 215–270 (1963)

Pickens, J.F., Grisak, G.E.: Scale-dependent dispersion in a stratified granular aquifer. Water Resour. Res. 17, 1191–1211 (1981)

Press, W.H., Teukolsky, S.A., Vetterling, W.T., Flannery, B.P.: Numerical Recipes in C: the Art of Scientific Computing, 2nd Edition. Cambridge Univ. Press, New York (1992)

Sahimi, M.: Flow phenomena in rocks: from continuum models to fractals, percolation, cellular automata, and simulated annealing. Rev. Modern Phys. 65, 1393–1534 (1993)

Sen, P.N., Goode, P.A.: Influence of temperature on electrical conductivity of shaly sands. Geophysics 57, 89–96 (1992)

Six, P.: Contribution à l'étude de la perméabilité d'une roche poreuse à un liquide. Rev. Inst. Fr. Pét. 17, 1454–1472 (1962)

387 Taylor, G.: Dispersion of soluble matter in solvent flowing slowly through a tube. Proc. Royal.
388 Soc. Ser. A 219, 186–203 (1953)
389 Xu, M.J., Eckstein, Y.: Use of weighted least-squares method in evaluation of the relationship
390 between dispersivity and field-scale. Ground Water 33, 905–908 (1995)
391

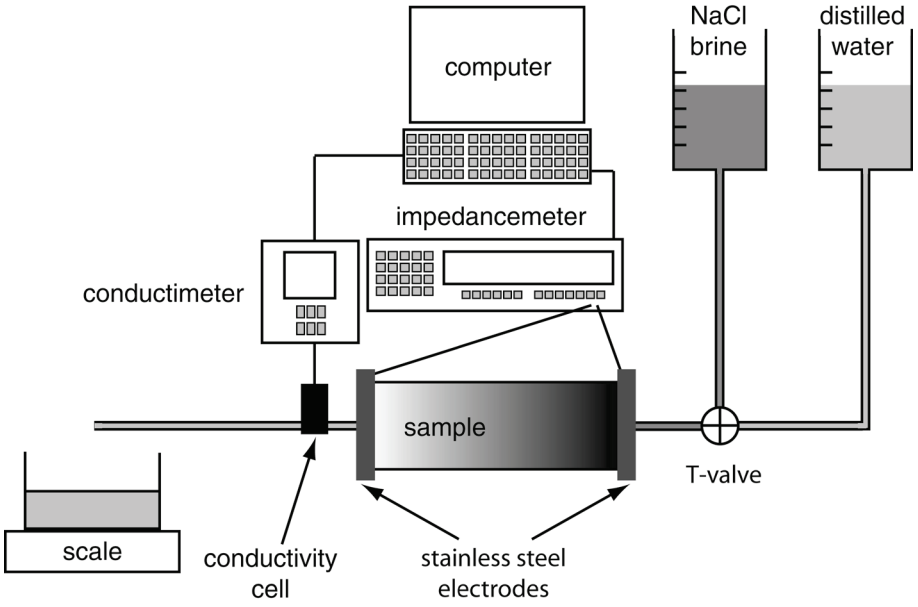

392

393 **Fig. 1.** Scheme of the experimental device for miscible displacement. Explanation in the text.

394

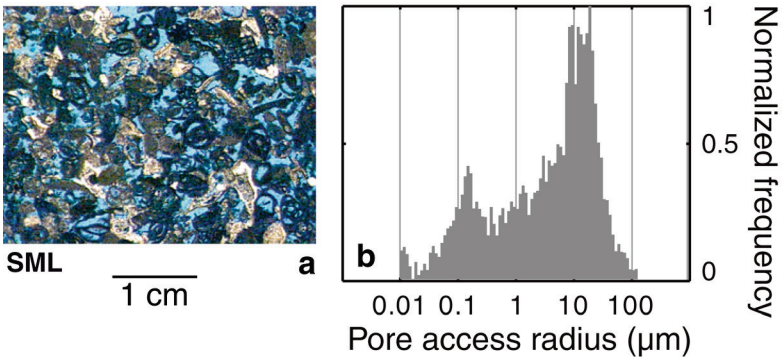

395

396 **Fig. 2.** (a) Thin section of Saint-Maximin limestone SML, where the blue areas correspond to the

397 void space filled by the resin; (b) histogram of pore access radius distribution inferred from

398 mercury injection.

399

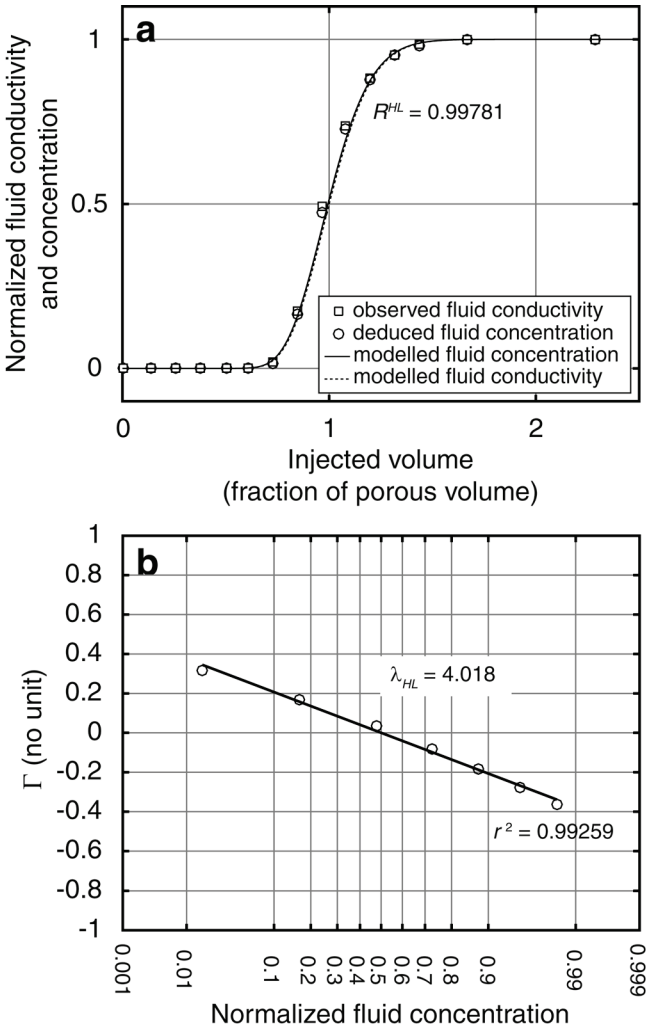

400

401 **Fig. 3.** Determination of the dispersivity by fitting the conductivity of the outflowing fluid in
402 Henry's space for Saint-Maximin limestone SML. (a) Observed fluid conductivity and deduced
403 fluid concentration (squares and circles), as a function of the injected volume of brine expressed
404 in fraction of total porous volume; (b) concentration in Henry's space (see text for detail). The
405 dispersivity value $\lambda_{HL} = 4.018$ mm, deduced from the slope of the line, is then used to model the
406 fluid concentration and conductivity shown by the lines in (a). R^{HL} is the value of the cost-
407 function.

408

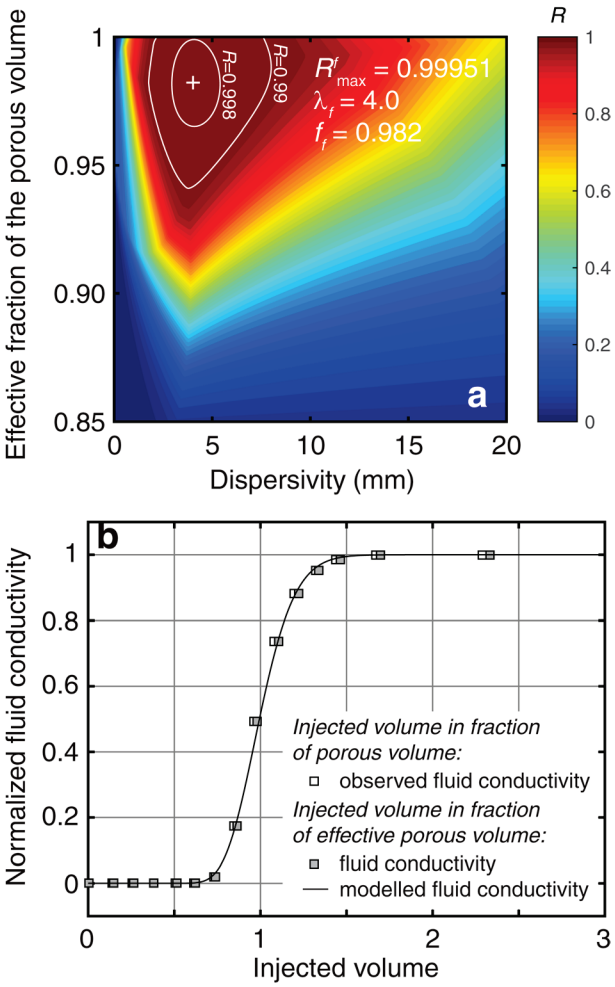

409

410 **Fig. 4.** Exploration of the parameter space to model the evolution of the outflowing fluid

411 conductivity for Saint-Maximin limestone SML. (a) isocontours of the cost-function R^f as a

412 function of the dispersivity and the effective fraction; (b) optimal solution (λ_f = 4 mm and

413 f_f = 0.982).

414

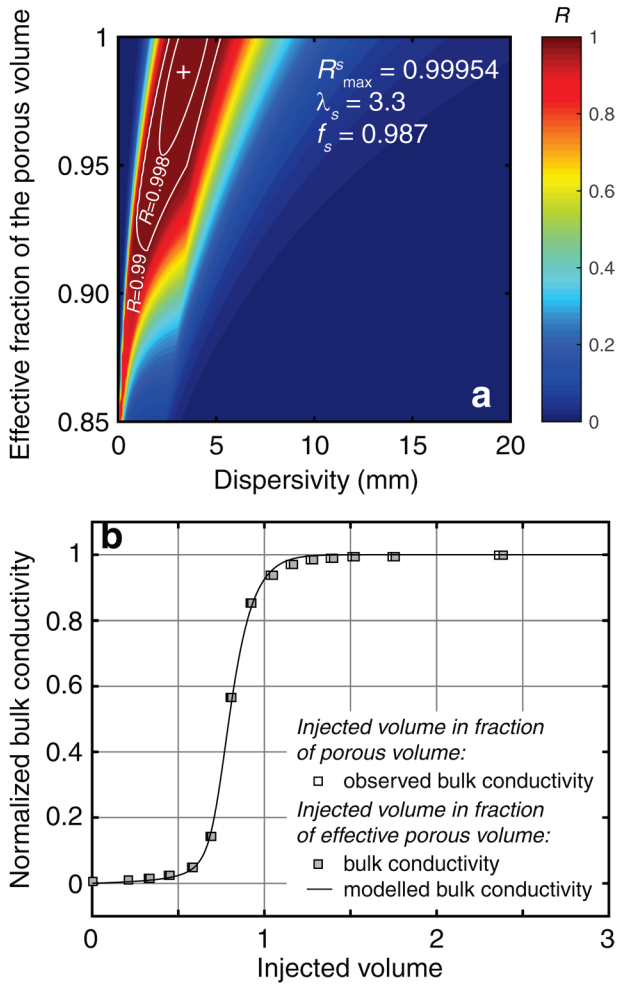

415

416 **Fig. 5.** Exploration of the parameter space to model the evolution of the bulk conductivity of the
417 SML sample. (a) isocontours of the cost-function R^s as a function of the dispersivity and the
418 effective fraction; (b) optimal solution (λ_f = 3.3 mm and f_f = 0.987). Note that the cost-function R^s
419 is more sensitive to the variations of the dispersivity than R^f, but globally less sensitive to the
420 variations of the effective fraction (compare to Figure 5).

421

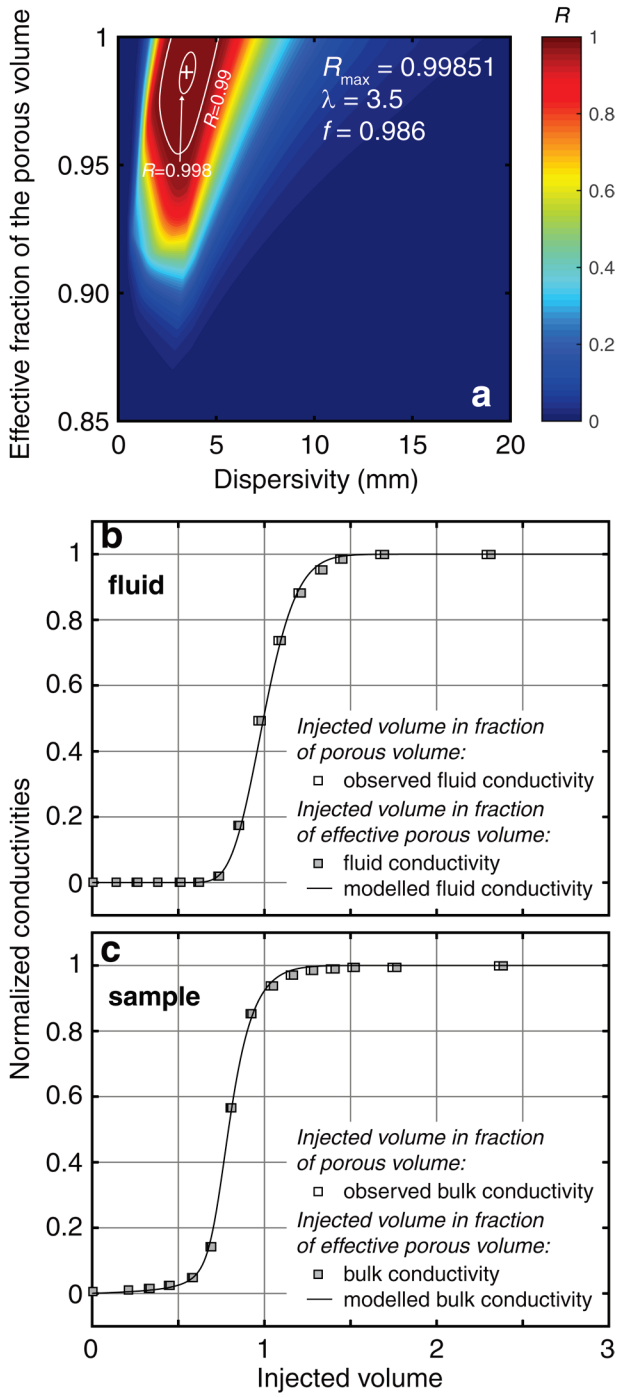

422

423 **Fig. 6.** Exploration of the parameter space to model simultaneously the evolutions of the

424 outflowing fluid and bulk conductivities for the SML sample. (a) isocontours of the cost-function

425 R as a function of the dispersivity and the effective fraction; (b) and (c) optimal solution ($\lambda = 3.5$

426 mm and $f = 0.986$).